Nuclear data measurements at the upgraded neutron time-of-flight facility n_TOF at CERN

F. Gunsing[1,2], O. Aberle[1], J. Andrzejewski[3], L. Audouin[4], V. Bécares[5], M. Bacak[6], J. Balibrea-Correa[5], M. Barbagallo[7], S. Barros[8], F. Bečvář[9], C. Beinrucker[10], F. Belloni[2], E. Berthoumieux[2], J. Billowes[11], D. Bosnar[12], M. Brugger[1], M. Caamaño[13], F. Calviño[14], M. Calviani[1], D. Cano-Ott [5], R. Cardella[1], D. M. Castelluccio[15,16], F. Cerutti[1], Y. Chen[4], E. Chiaveri[1], N. Colonna[7], M. A. Cortés-Giraldo[17], G. Cortés[14], L. Cosentino[18], L. Damone[7], K. Deo[19], M. Diakaki[2], C. Domingo-Pardo[20], R. Dressler[21], E. Dupont[2], I. Durán[13], B. Fernández-Domínguez[13], A. Ferrari[1], P. Ferreira[8], P. Finocchiaro[18], R. J. W. Frost[11], V. Furman[22], S. Ganesan[19], A. Gawlik[3], I. Gheorghe[23], T. Glodariu[23], I. F. Gonçalves[8], E. González[5], A. Goverdovski[24], E. Griesmayer[6], C. Guerrero[17], K. Göbel[10], H. Harada[25], T. Heftrich[10], S. Heinitz[21], A. Hernández-Prieto[1,14], J. Heyse[26], G. Jenkins[27], E. Jericha[6], F. Käppeler[28], Y. Kadi[1], T. Katabuchi[29], P. Kavrigin[6], V. Ketlerov[24], V. Khryachkov[24], A. Kimura[25], N. Kivel[21], M. Kokkoris[30], M. Krtička[9], E. Leal-Cidoncha[13], C. Lederer[31,10], H. Leeb[6], J. Lerendegui[17], M. Licata[16,32], S. Lo Meo[15,16], R. Losito[1], D. Macina[1], J. Marganiec[3], T. Martínez[5], C. Massimi[16,32], P. Mastinu[33], M. Mastromarco[7], F. Matteucci[34], E. A. Maugeri[21], E. Mendoza[5], A. Mengoni[15], P. M. Milazzo[34], F. Mingrone[16], M. Mirea[23], S. Montesano[1], A. Musumarra[18], R. Nolte[35], A. Oprea[23], F. R. Palomo Pinto[17], C. Paradela[13], N. Patronis[36], A. Pavlik[37], J. Perkowski[3], J. I. Porras[1,38], J. Praena[17], J. M. Quesada[17], T. Rauscher[39,40], R. Reifarth[10], A. Riego-Perez[14], M. Robles[13], C. Rubbia[1], J. A. Ryan[11], M. Sabaté-Gilarte[1,17], A. Saxena[19], P. Schillebeeckx[26], S. Schmidt[10], D. Schumann[21], P. Sedyshev[22], A. G. Smith[11], A. Stamatopoulos[30], S. V. Suryanarayana[19], G. Tagliente[7], J. L. Tain[20], A. Tarifeño-Saldivia[20], L. Tassan-Got[4], A. Tsinganis[30], S. Valenta[9], G. Vannini[16,32], V. Variale[7], P. Vaz[8], A. Ventura[16], V. Vlachoudis[1], R. Vlastou[30], A. Wallner[41], S. Warren[11], M. Weigand[10], C. Weiss[1,6], C. Wolf[10], P. J. Woods[31], T. Wright[11], P. Žugec[12,1], The n_TOF Collaboration

Abstract

Applications of nuclear data like neutron-induced reaction cross sections are related to research fields as stellar nucleosynthesis, the study of nuclear level densities and strength functions, and also play a key role in the safety and criticality assessment of existing and future nuclear reactors, in areas concerning radiation dosimetry, medical applications, transmutation of nuclear waste, accelerator-driven systems and fuel cycle investigations. The evaluations in nuclear data libraries are based both on experimental data and theoretical models. CERN's neutron time-of-flight facility n_TOF has produced a considerable amount of experimental data since it has become fully operational with the start of its scientific measurement programme in 2002. While for a long period a single measurement station (EAR1) located at 185 m from the neutron production target was available, the construction of a second beam line at 20 m (EAR2) in 2014 has substantially increased the measurement capabilities of the facility. An outline of the experimental nuclear data activities at CERN's neutron time-of-flight facility n_TOF will be presented.

1. Introduction

Nuclear data is a generic notion comprising the physical properties related to nuclear structure and nuclear reactions. Evaluated nuclear reaction data are intended to be complete and to contain all reactions and all energy regions, even where experimental data are missing, insufficient or inconsistent with other experimental data sets. A nuclear data evaluation is a complicated process resulting from a careful

analysis of available existing, sometimes inconsistent experimental data sets combined with optimum theoretical models describing experimental data and providing data for gaps in experimental information. The outcome of this process is a single recommended dataset, the evaluation. Both theoretical models and experimental data are the fundamental ingredients in evaluated data.

Nuclear data in general, and neutron-induced reactions in particular, are important for a number of research fields. They play a key role in the safety and criticality assessment of nuclear technology, not only for existing power reactors but also for medical applications [1], radiation dosimetry, the transmutation of nuclear waste, accelerator-driven systems, future reactor systems as in Generation IV, and the thorium-based nuclear fuel cycle [2, 3, 4]. Other applications of nuclear data are related to research fields as the study of nuclear level densities [5, 6] and stellar nucleosynthesis [7, 8, 9].

The nuclear data of nuclear reactions needed for such calculations are usually based on evaluated nuclear data libraries, like JEFF [10], ENDF [11], JENDL [12], CENDL, BROND and several others. Contributions to nuclear data come from a variety of experimental facilities, including the pulsed white neutron source n_TOF at CERN, which has been recently upgraded with a second beam line.

2.   The neutron time-of-flight facility n_TOF at CERN

The neutron time-of-flight facility n_TOF was constructed after an idea proposed by Rubbia *et al.*[45] and has become fully operational with the start of the scientific measurement programme in May 2002. The facility is based on the 6 ns wide, 20 GeV/*c* pulsed proton beam from CERN's Proton Synchrotron (PS) with typically 7×10^{12} protons per pulse, impinging on a lead spallation target, yielding about 300 neutrons per incident proton. A layer of water around the spallation target moderates the initially fast neutrons down to a white spectrum of neutrons covering the full range between meV and GeV neutron energy. The minimal time between two proton pulses is a multiple of 1.2 s, related to the operation cycle of the PS. This allows to cover the neutron energy range down to subthermal energies without overlap of slow neutrons from previous cycles.

During phase-I when the first spallation target was used from 2001 up to 2004, the water coolant also served as the moderator. The spallation target was a block of lead of dimensions $80 \times 80 \times 60$ cm^3. During phase-II, after the installation in 2008 of an upgraded cylindrical lead spallation target 60 cm in length and 40 cm in diameter, the target was enclosed with a separate cooling circuit resulting in a 1 cm water layer in the beam direction, followed by an exchangeable moderator with a thickness of 4 cm. Normal water has been used as a moderator, as well as water with a saturated ^{10}B-solution in order to reduce the number of 2.23 MeV gamma rays from hydrogen capture, which otherwise forms an important contribution to the background due to in-beam gamma rays. The ^{10}B-loaded moderator affects the energy distribution of the neutron flux only noticeably below 1 eV. The kinetic energy of the neutrons is determined by time-of-flight which, combined with the known flight distance, gives the neutron velocity.

A first neutron beam is collimated and guided through a vacuum neutron tube over a distance of approximately 185 m to an experimental area (EAR1) where samples can be mounted in the beam and neutron induced reactions can be studied. A more detailed description of the neutron source and EAR1 can be found in Ref. [46] and references therein.

A second neutron beam line and experimental area (EAR2), sketched in Fig. 1 has been constructed and is operational since 2014. This flight path is vertical and about 20 m long, viewing the top part of the spallation target. In this case the cooling water circuit acts as a moderator. Due to the about 10 times shorter flight length, a much higher neutron flux of about a factor 25 is available, as shown in Fig. 2. The about 10 times shorter flight path implies also in about 10 times shorter flight times,

Table 1: The measurements performed at n_TOF during phase-I from 2001-2004.

nucleus	reaction	detector	ref.	nucleus	reaction	detector	ref.
^{24}Mg	(n,γ)	C_6D_6	[13]	^{232}Th	(n,γ)	C_6D_6	[30, 31]
^{26}Mg	(n,γ)	C_6D_6	[13]	^{233}U	(n,γ)	TAC	
^{90}Zr	(n,γ)	C_6D_6	[14]	^{234}U	(n,γ)	TAC	
^{91}Zr	(n,γ)	C_6D_6	[15]	^{237}Np	(n,γ)	TAC	[32]
^{92}Zr	(n,γ)	C_6D_6	[16]	^{240}Pu	(n,γ)	TAC	
^{94}Zr	(n,γ)	C_6D_6	[17]	^{243}Am	(n,γ)	TAC	[33]
^{96}Zr	(n,γ)	C_6D_6	[18]	^{233}U	(n,f)	FIC	[34, 35]
^{129}La	(n,γ)	C_6D_6	[19]	^{234}U	(n,f)	FIC	[36]
^{151}Sm	(n,γ)	C_6D_6	[20, 21, 22]	^{236}U	(n,f)	FIC	[37]
^{186}Os	(n,γ)	C_6D_6	[23, 24]	^{241}Am	(n,f)	FIC	[38]
^{187}Os	(n,γ)	C_6D_6	[23, 24]	^{243}Am	(n,f)	FIC	[39]
^{188}Os	(n,γ)	C_6D_6	[23, 24]	^{245}Cm	(n,f)	FIC	[40]
^{204}Pb	(n,γ)	C_6D_6	[25]	^{234}U	(n,f)	PPAC	[41, 42]
^{206}Pb	(n,γ)	C_6D_6	[26, 27]	^{237}Np	(n,f)	PPAC	[41]
^{207}Pb	(n,γ)	C_6D_6	[28]	^{209}Bi	(n,f)	PPAC	[43]
^{208}Pb	(n,γ)	C_6D_6		^{nat}Pb	(n,f)	PPAC	[43]
^{209}Bi	(n,γ)	C_6D_6	[29]	^{232}Th	(n,f) ang.	PPAC	[44]

resulting in an additional factor 10 gain in the signal to noise ratio due to radioactivity. More details on EAR2 can be found in Refs. [47, 48].

2.1 Nuclear data measurements during phase-I (2001-2004)

During the first phase from 2001 to 2004 capture and fission data for a number of isotopes have been taken. Capture measurements with C_6D_6 liquid scintillator detectors concerned ^{24,25,26}Mg, ^{56}Fe, the stable isotopes ^{90,91,92,94,96}Zr and the radioactive one ^{93}Zr, as well as the nuclei ^{139}La, ^{151}Sm, ^{186,187,188}Os, ^{197}Au, ^{204,206,207,208}Pb, ^{209}Bi, and ^{232}Th. A 4π calorimeter consisting of 40 BaF$_2$ crystals has been used for neutron capture measurements of ^{197}Au, ^{233}U, ^{234}U, and ^{237}Np, ^{240}Pu, and ^{243}Am. Fission cross sections were measured with the FIC-0 fission detector containing the actinides ^{232}Th, ^{234}U, ^{235}U, ^{236}U, ^{238}U, and ^{237}Np. A similar detector, FIC-1, which was ISO-2919 compliant, was used to measure neutron-induced fission cross sections of the actinides ^{233}U, ^{235}U, ^{238}U ^{241}Am, ^{243}Am, and ^{245}Cm. Fission detectors based on Parallel Plate Avalanche Counters (PPACs) were developed and used in measurements of the fission cross sections of ^{nat}Pb, ^{209}Bi, ^{232}Th, ^{237}Np, ^{233}U, ^{234}U, ^{235}U and ^{238}U. A list of measured isotopes and reactions together with the final or most relevant publication is given in table 1.

2.2 Nuclear data measurements during phase-II (2009-2012)

During phase-II from 2009-2012 mostly capture measurements were performed. The (n,γ) reaction on the light nucleus ^{25}Mg was investigated, as well as on several enriched iron and nickel isotopes (^{54}Fe, ^{56}Fe, ^{57}Fe, ^{58}Ni, ^{62}Ni, ^{63}Ni), and on the stable ^{92}Zr and radioactive ^{93}Zr. Capture reactions on the actinides ^{236}U, ^{238}U and ^{241}Am were performed, for the latter two with two different capture detector systems: C_6D_6 scintillators using the total energy method, and the TAC, the BaF$_2$ scintillator array using the total absorption method. The TAC was also used in combination with a MicroMegas detector in a first attempt to measure the ^{235}U(n,γ) reaction using a veto on the ^{235}U(n,f) reaction.

Table 2: The measurements performed at n_TOF during phase-II from 2009-2012.

nucleus	reaction	detector	ref.
^{33}S	(n,α)	MGAS	
^{59}Ni	(n,α)	CVD	[49]
^{25}Mg	(n,γ)	C_6D_6	[50]
^{54}Fe	(n,γ)	C_6D_6	[51]
^{56}Fe	(n,γ)	C_6D_6	
^{57}Fe	(n,γ)	C_6D_6	[51]
^{58}Ni	(n,γ)	C_6D_6	[52]
^{62}Ni	(n,γ)	C_6D_6	[53]
^{63}Ni	(n,γ)	C_6D_6	[54]
^{87}Sr	(n,γ) spin	TAC	[55]
^{92}Zr	(n,γ)	C_6D_6	

nucleus	reaction	detector	ref.
^{93}Zr	(n,γ)	C_6D_6	[56]
^{197}Au	(n,γ)	C_6D_6/TAC	[57, 58]
^{235}U	(n,γ)/(n,f)	TAC/MGAS	[59]
^{236}U	(n,γ)	C_6D_6	[60]
^{238}U	(n,γ)	C_6D_6	[61]
^{238}U	(n,γ)	TAC	[62]
^{241}Am	(n,γ)	C_6D_6	[63]
^{241}Am	(n,γ)	TAC	[64]
^{242}Pu	(n,f)	MGAS	[65]
^{12}C	(n,p) activ.	C_6D_6	[66, 67]

In addition to these measurements several other techniques have been tested at this facility. An experiment aiming at resonance spin assignments was performed on a ^{87}Sr sample. A first test measurement with a MicroMegas detector was done to perform a fission measurement on ^{240}Pu and ^{242}Pu. The results on ^{240}Pu(n,f) were not conclusive due to the high radioactivity of this nucleus, degrading the detector over time. This measurement was repeated in 2014 in the new EAR2, where the flux is much higher, allowing to collect enough statistics in only a few weeks of measurement time. Another reaction that was investigated was the ^{33}S(n,α) reaction with a MicroMegas detector. Also this measurement was was repeated later in EAR2 in 2015 to take advantage of the higher flux. A CVD diamond detector was used to measure the ^{59}Ni(n,α) cross section. Finally the ^{12}C(n,p)^{12}B reaction was exploited by in-beam activation [67]. A list of the phase-II measurements and their references are given in table 2.

2.3 Nuclear data measurements during phase-III (from 2014)

During the long planned shutdown of CERN's accelerator complex from the end of 2012 to mid 2014, the construction of n_TOF's new second beam line and experimental area EAR2 [68] was performed and delivered by July 2014. The design was based on extensive Monte Carlo simulations with FLUKA [48] in order to optimize the beam line and collimation for a high neutron flux together with a minimized background. An impression of the EAR2 is shown in fig. 1. In order to remove charged particles from the beam, a permanent 0.25 T magnet had to be installed since unlike the beamline for EAR1, there was no room for an electromagnet. Since then, the facility has been taking data in both the experimental area EAR1 (185 m horizontal flight path), and in the new EAR2 (20 m vertical flight path), using the neutron beams simultaneously produced by the same cylindrical lead spallation target as used in Phase-II.

For the operation of Phase-III, a new data acquisition system was developed, based on 175 MSample digitizers with 1 ns of time-, and 12 bit amplitude resolution. In addition to the higher-amplitude resolution, which was 8 bits with the previously used digitizers, a larger on-board memory allows now to expand the exploitable time-of-flight range down to thermal neutron energies.

A set of in-house designed C_6D_6-based gamma-ray detectors and newly designed neutron flux detectors based on silicon detectors and MicroMegas detectors [69] were used in beam. An XY-MircoMegas detector with dedicated electronics was developed to measure the neutron beam profile.

The measurement programme in EAR2 started with a first part of commissioning by measuring the elementary quantities as flux and background and focussing on the feasibility of fission measurements. The energy dependence of the number of neutrons incident on the sample, approximatively re-
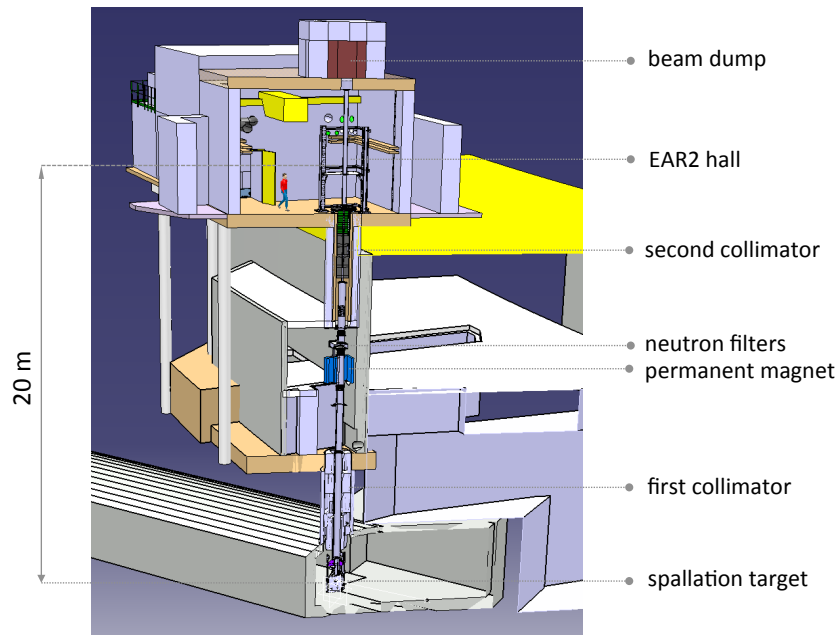
Fig. 1: Impression of n_TOF EAR2 from the spallation target up to the experimental hall.
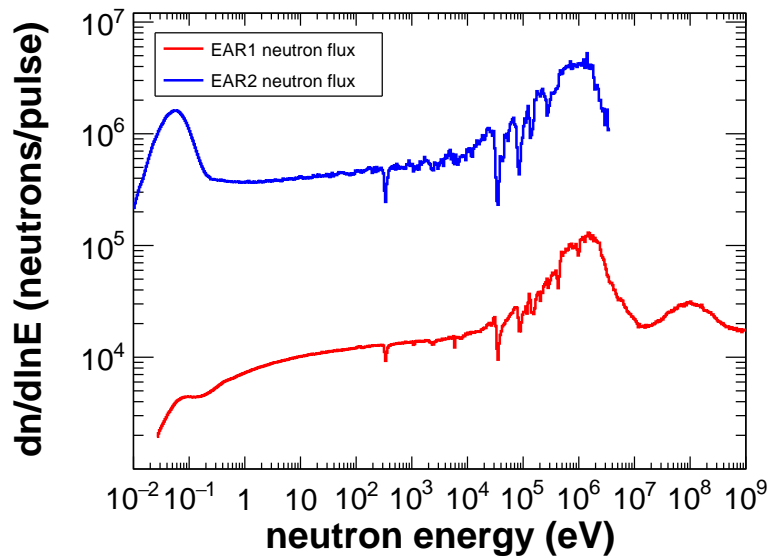

Fig. 2: The number of neutrons per equidistant logarithmic energy bin (dn/dlnE) per 7×12 protons on target, as seen at the sample position at nominal distances of 185 m (EAR1) and 20 m (EAR2). The shown fluxes are the preliminary results of several measurements and simulations.

ferred to as the neutron flux, was measured both with an in-beam neutron-to-charged-particle converter foil, monitored by off-beam silicon detectors, and foils combined with in-beam MicroMegas detectors. The neutron converters consisted of isotopes with well known reactions as ^{6}Li(n,α), ^{10}B(n,α) and ^{235}U(n,f) in order to cover the energy dependence over a broad energy range. In fig. 2 the measured

Table 3: The nuclear data measurements performed at n_TOF during phase-III in 2014 and 2015 for both EAR1 and EAR2.

nucleus	reaction	detector	EAR	ref.
^{70}Ge	(n,γ)	C_6D_6	EAR1	
^{73}Ge	(n,γ)	C_6D_6	EAR1	
^{74}Ge	(n,γ)	C_6D_6	EAR1	
^{76}Ge	(n,γ)	C_6D_6	EAR1	
^{171}Tm	(n,γ)	C_6D_6	EAR1, EAR2	
^{204}Tl	(n,γ)	C_6D_6	EAR1	
^{242}Pu	(n,γ)	C_6D_6	EAR1	
^{237}Np	(n,f)	PPAC	EAR1	
^{33}S	(n,α)	MGAS	EAR2	
^{7}Be	(n,α)	MGAS	EAR2	
^{240}Pu	(n,f)	MGAS	EAR2	[70]
^{147}Pm	(n,γ)	C_6D_6	EAR2	
^{235}U	(n,f)FF	STEFF	EAR2	

neutron fluxes in EAR1 and EAR2 are shown. The thermal peak is strongly suppressed for EAR1 due to the addition of ^{10}B in the separate moderator. The thermal flux in EAR2 is not affected because in this direction only the cooling water acts as a moderator.

After the first part of commissioning, the very first physics measurement in EAR2 concerned the ^{240}Pu(n,f) reaction with MicroMegas detectors [70]. In 2015, the commissioning of EAR2 continued, exploring the possibilities of (n,γ) measurements, for applications in nuclear astrophysics [71] and nuclear technology, as well as neutron-induced charged particle reactions like the ^{7}Be(n,α) and upcoming ^{7}Be(n,p) experiments. A list of measurements during 2014 and 2015 and their references are given in table 3.

Conclusion

The key features of the n_TOF facility with its two beam lines and experimental areas EAR1 and EAR2 are a large energy range, high neutron-energy resolution, and a high instantaneous neutron flux. EAR2 with its about 25 times higher flux than in EAR1, combined with an additional reduction by a factor 10 of the background due to radioactivity, significantly enhances the possible measurements on unstable targets at n_TOF. The preparation and characterization of such targets suitable for neutron cross-section measurements is an increasingly complicated task, feasible only in highly specialized laboratories.

References

[1] S. M. Qaim. *Radiochimica Acta*, **101**(8):473–480, 2013.
[2] G. Aliberti, G. Palmiotti, M. Salvatores, et al. *Nuclear Science and Engineering*, **146**(1):13–50, 2004.
[3] A. Nuttin, D. Heuer, A. Billebaud, et al. *Progress In Nuclear Energy*, **46**(1):77–99, 2005.
[4] A. Nuttin, P. Guillemin, A. Bidaud, et al. *Annals of Nuclear Energy*, **40**(1):171–189, 2012.
[5] T. von Egidy and D. Bucurescu. *Phys. Rev. C*, **73**(4):049901, 2006.
[6] H. A. Weidenmuller and G. E. Mitchell. *Rev. Mod. Phys.*, **81**(2):539–589, 2009.
[7] S. E. Woosley, A. Heger, T. Rauscher, et al. *Nucl. Phys. A*, **718**:3C–12C, 2003.
[8] F. Käppeler, R. Gallino, S. Bisterzo, et al. *Rev. Mod. Phys.*, **83**(1):157–193, 2011.
[9] T. Rauscher. *Aip Advances*, **4**(4):041012, 2014.
[10] A. J. Koning, E. Bauge, C. J. Dean, et al. *J. Korean Phys. Soc.*, **59**(2):1057–1062, 2011.

[11] M. B. Chadwick, M. Herman, P. Oblozinsky, et al. *Nucl. Data Sheets*, **112**(12):2887–2996, 2011.

[12] K. Shibata. *J. Nucl. Sci. Tech.*, **50**(5):449–469, 2013.

[13] C. Massimi, P. Koehler, S. Bisterzo, et al. *Phys. Rev. C*, **85**(4):044615, 2012.

[14] G. Tagliente, K. Fujii, P. M. Milazzo, et al. *Phys. Rev. C*, **77**(3):035802, 2008.

[15] G. Tagliente, P. M. Milazzo, K. Fujii, et al. *Phys. Rev. C*, **78**(4):045804, 2008.

[16] G. Tagliente, P. M. Milazzo, K. Fujii, et al. *Phys. Rev. C*, **81**(5):055801, 2010.

[17] G. Tagliente, P. M. Milazzo, K. Fujii, et al. *Phys. Rev. C*, **84**(1):015801, 2011.

[18] G. Tagliente, P. M. Milazzo, K. Fujii, et al. *Phys. Rev. C*, **84**(5):055802, 2011.

[19] R. Terlizzi, U. Abbondanno, G. Aerts, et al. *Phys. Rev. C*, **75**(3):035807, 2007.

[20] U. Abbondanno, G. Aerts, F. Alvarez-Velarde, et al. *Phys. Rev. Lett.*, **93**(16):161103, 2004.

[21] S. Marrone, U. Abbondanno, G. Aerts, et al. *Nucl. Phys. A*, **758**:533C–536C, 2005.

[22] S. Marrone, U. Abbondanno, G. Aerts, et al. *Phys. Rev. C*, **73**(3):034604, 2006.

[23] K. Fujii, M. Mosconi, A. Mengoni, et al. *Phys. Rev. C*, **82**(1):015804, 2010.

[24] M. Mosconi, K. Fujii, A. Mengoni, et al. *Phys. Rev. C*, **82**(1):015802, 2010.

[25] C. Domingo-Pardo, U. Abbondanno, G. Aerts, et al. *Phys. Rev. C*, **75**(1):015806, 2007.

[26] C. Domingo-Pardo, U. Abbondanno, G. Aerts, et al. *Phys. Rev. C*, **76**(4):045805, 2007.

[27] C. Domingo-Pardo, U. Abbondanno, G. Aerts, et al. *J. Phys. G*, **35**(1):014020, 2008.

[28] C. Domingo-Pardo, U. Abbondanno, G. Aerts, et al. *Phys. Rev. C*, **74**(5):055802, 2006.

[29] C. Domingo-Pardo, U. Abbondanno, G. Aerts, et al. *Phys. Rev. C*, **74**(2):025807, 2006.

[30] G. Aerts, U. Abbondanno, H. Alvarez, et al. *Phys. Rev. C*, **73**(5):054610, 2006.

[31] F. Gunsing, E. Berthoumieux, G. Aerts, et al. *Phys. Rev. C*, **86**(1):019902, 2012.

[32] C. Guerrero, D. Cano-Ott, E. Mendoza, et al. *Phys. Rev. C*, **85**(4):044616, 2012.

[33] E. Mendoza, D. Cano-Ott, C. Guerrero, et al. *Phys. Rev. C*, **90**(3):034608, 2014.

[34] M. Calviani, J. Praena, U. Abbondanno, et al. *Phys. Rev. C*, **80**(4):044604, 2009.

[35] F. Belloni, M. Calviani, N. Colonna, et al. *Eur. Phys. J. A*, **47**(1):2, 2011.

[36] D. Karadimos, R. Vlastou, K. Ioannidis, et al. *Phys. Rev. C*, **89**(4):044606, 2014.

[37] R. Sarmento, M. Calviani, J. Praena, et al. *Phys. Rev. C*, **84**(4):044618, 2011.

[38] F. Belloni, M. Calviani, N. Colonna, et al. *Eur. Phys. J. A*, **49**(1):2, 2013.

[39] F. Belloni, M. Calviani, N. Colonna, et al. *Eur. Phys. J. A*, **47**(12):160, 2011.

[40] M. Calviani, M. H. Meaze, N. Colonna, et al. *Phys. Rev. C*, **85**(3):034616, 2012.

[41] C. Paradela, L. Tassan-Got, L. Audouin, et al. *Phys. Rev. C*, **82**(3):034601, 2010.

[42] E. Leal-Cidoncha, I. Duràn, C. Paradela, et al. *Nucl. Data Sheets*, **119**(0):42 – 44, 2014.

[43] D. Tarrio, L. Tassan-Got, L. Audouin, et al. *Phys. Rev. C*, **83**(4):044620, 2011.

[44] D. Tarrio, L. S. Leong, L. Audouin, et al. *Nucl. Instr. Meth. A*, **743**:79–85, 2014.

[45] C. Rubbia et al. "a high resolution spallation driven facility at the CERN-PS to measure neutron cross sections in the interval from 1 eV to 250 MeV". Technical report, 1998.

[46] C. Guerrero, A. Tsinganis, E. Berthoumieux, et al. *Eur. Phys. J. A*, **49**(2):27, 2013.

[47] C. Weiss, , et al. The new vertical neutron beam line at the {CERN} n_TOF facility design and outlook on the performance. *Nucl. Instr. Meth. A*, **799**:90 – 98, 2015.

[48] S. Barros, I. Bergström, V. Vlachoudis, C. Weiss, and n_TOF collaboration. Optimization of n_TOF-EAR2 using FLUKA. *Journal of Instrumentation*, **10**(09):P09003, 2015.

[49] C. Weiss, C. Guerrero, E. Griesmayer, et al. *Nucl. Data Sheets*, **120**(0):208 – 210, 2014.

[50] C. Massimi, P. Koehler, F. Mingrone, et al. *Nucl. Data Sheets*, **119**(0):110 – 112, 2014.

[51] G. Giubrone, C. Domingo-Pardo, J.L. Taín, et al. *Nucl. Data Sheets*, **119**(0):117 – 120, 2014.

[52] P. Žugec, M. Barbagallo, N. Colonna, et al. *Phys. Rev. C*, **89**(1):014605, 2014.

[53] C. Lederer, C. Massimi, E. Berthoumieux, et al. *Phys. Rev. C*, **89**(2):025810, 2014.

[54] C. Lederer, C. Massimi, S. Altstadt, et al. *Phys. Rev. Lett.*, **110**(2):022501, 2013.

[55] F. Gunsing, K. Fraval, M. Mathelie, et al. *Nucl. Data Sheets*, **119**(0):132 – 136, 2014.

[56] G. Tagliente, P. M. Milazzo, K. Fujii, et al. *Phys. Rev. C*, **87**(1):014622, 2013.

[57] C. Massimi, C. Domingo-Pardo, G. Vannini, et al. *Phys. Rev. C*, **81**(4):044616, 2010.

[58] C. Lederer, N. Colonna, C. Domingo-Pardo, et al. *Phys. Rev. C*, **83**(3):034608, 2011.

[59] J. Balibrea, E. Mendoza, D. Cano-Ott, et al. *Nucl. Data Sheets*, **119**(0):10 – 13, 2014.

[60] M. Barbagallo, N. Colonna, M.J. Vermeulen, et al. *Nucl. Data Sheets*, **119**(0):45 – 47, 2014.

[61] F. Mingrone, C. Massimi, S. Altstadt, et al. *Nucl. Data Sheets*, **119**(0):18 – 21, 2014.

[62] T. Wright, C. Guerrero, J. Billowes, et al. *Nucl. Data Sheets*, **119**(0):26 – 30, 2014.

[63] K. Fraval, F. Gunsing, S. Altstadt, et al. *Phys. Rev. C*, **89**(4):044609, 2014.

[64] E. Mendoza, D. Cano-Ott, C. Guerrero, et al. *Nucl. Data Sheets*, **119**(0):65 – 68, 2014.

[65] A. Tsinganis, E. Berthoumieux, C. Guerrero, et al. *Nucl. Data Sheets*, **119**(0):58 – 60, 2014.

[66] P. Žugec, N. Colonna, D. Bosnar, et al. *Phys. Rev. C*, **90**(2):021601, 2014.

[67] P. Žugec et al. *These proceedings*, 2015.

[68] E. Chiaveri et al. "Proposal for n_TOF experimental area 2". Technical report, 2011.

[69] F. Belloni, , et al. "Micromegas for neutron detection and imaging". *Mod. Phys. Lett. A*, **28**, 13 (2013) 1340023

[70] A. Tsinganis et al. *These proceedings*, 2015.

[71] G. Tagliente et al. *These proceedings*, 2015.